JOURNAL OF GUIDANCE, CONTROL, AND DYNAMICS
Vol. 18, No. 2, March–April 1995

Covariance Control Design for Hubble Space Telescope

Guoming Zhu,* Karolos M. Grigoriadis,† and Robert E. Skelton‡
Purdue University, West Lafayette, Indiana 47907

To improve the response to unexpected thermally induced disturbances, two new controllers are designed for the Hubble Space Telescope (HST) using covariance control techniques. The first controller minimizes the required control effort subject to inequality constraints on the output covariance matrix. The second controller is designed to satisfy both output covariance constraints and controller covariance constraints. The importance of the controller covariance constraint is to properly scale the controller for digital implementation in the control computer using fixed-point arithmetic. We provide a technique to integrate modeling, control design, and signal processing (in HST's fixed-point control computer), since these problems are not separable. Covariance control can easily accommodate the roundoff error and computational time delay. Compared with the existing HST controller design, the results show that the required pointing error specifications can be achieved with 85% less control effort and that the error due to the finite-wordlength implementation of the controller can easily be included in the optimal control design process.

Introduction

THE Hubble Space Telescope (HST) is an orbiting, 2.4-m-diam Ritchie-Critien-type Cassegrainian telescope that is operated as an international astronomical facility. After the launch on April 25, 1990, unexpected large disturbances degraded the pointing performance of the HST. The analysis of the flight data and simulation results suggest that the disturbance is caused by thermally excited dynamics in the solar panel bistems.

The HST pointing control system (PCS) is a multirate, multiloop discrete-time system with multiple modes of operation. Each control loop of the existing design was designed and implemented as a single-input, single-output (SISO) compensator. A simplified overview of the PCS in the normal science mode can be found in Ref. 1. The vehicle coordinates (v_1, v_2, and v_3) are also defined in Ref. 1 and in Fig. 1. The pointing control requirements are to keep the angular rotational errors V_2 and V_3 about the axes v_2 and v_3, respectively, below 0.007 arc-s (in the sense that $\sup_{t\geq 0}[V_2^2(t) + V_3^2(t)]^{1/2} \leq 0.007$ in the presence of unknown disturbances given a bound on the energy). Vehicle rates are obtained from a skewed set of six integrated rate gyro assemblies (RGAs) whose signals are quantized using 12-bit analog-to-digital (A/D) conversion. These gyros have dual rate ranges. The low-rate range is utilized in the acquisition and science modes with a resolution of 1.25×10^{-4} arc-s per bit. The high-rate mode, which has a resolution of 0.0075 arc-s, automatically comes into play whenever the vehicle rates exceed 2 arc-s/s over a 5-s interval. Primary actuation is provided by four reaction wheel assemblies (RWAs). The spin axes of the RWAs are skewed relative to the HST vehicle frame to provide system redundancy. Thus, the PCS can operate with any three of the four reaction wheels by suitable construction of the vehicle-to-RWA transformation matrix. Each RWA has a maximum speed of 3000 rpm, 0.84 kg-m^2 rotor inertia, a torque bandwidth exceeding 50 Hz, and software-limited torque capability of 0.82 N-m.

The Space Systems Control Laboratory (SSCL) at Purdue was created in 1991 to develop a rapid redesign capability for space system controllers in flight. The HST is an ideal example of the need for such a facility. With a workstation environment the SSCL seeks to integrate an iterative procedure for identification, modeling, control design, and signal processing. It is well known that the modeling and control problems are not independent. In addition, the modeling and controller design should include integration of the signal processing issues, since the effects of finite precision controller computation can have unbounded effects on flight system performance.[2] That is, our design procedure will include the roundoff errors in the A/D, D/A, and flight computer in the formulation of the design problem. This will allow trade-offs of performance with computational resources. The main purpose of this paper is to present an integrated approach to these coupled problems (modeling, control design, and signal processing) to allow trade-off of performance against controller complexity (memory). The second objective of the paper is to apply our methodology to the HST. We have not attempted thorough comparisons with other designs.

The covariance control theory[3–6] is a natural control design methodology with which to integrate modeling, control, and signal processing issues, since both the effects of coefficient and state roundoff errors can easily be modeled in the covariance equations. The state-space realization of a system is invisible in a transfer function approach. Hence, input/output (transfer function) methods are powerless to treat the roundoff problem, which is a function of the state-space realization. Throughout this paper we take some literary license to refer to "variances" of the stochastic outputs (inputs) as root-mean-square (rms) values.

TREETOPS (the NASA-owned software for modeling n-connected rigid bodies) is used in this research, even though there are significant differences between TREETOPS models and the models identified using flight data.[7] Our integration of model reduction and control design is described in Fig. 2. First, modal cost analysis (MCA) is used for model reduction. An 83rd-order evaluation model and a 32nd-order design model are obtained by deleting the modes with small modal costs for the solar panel angles 0 deg, 45 deg, and 105 deg. Second, the output covariance constraint (OCC) design algorithm is applied to design a full-order dynamic controller based on the reduced-order model associated with the solar panel angle at 0 deg. Third, the alternating convex projection (ACP) algorithm[8] is used to find a feasible state covariance matrix satisfying all performance requirements. Using this covariance matrix, a covariance controller with minimal control effort is constructed to satisfy the design objectives. Finally, the finite-wordlength effects on the controller implementation are considered and evaluated. It is known in signal processing that there exists optimal coordinates[9] for realizing a controller with minimal roundoff error. Our results show that below 24 bits of control computer wordlength, transforming the controller coordinates to the optimal coordinates[2] (dictated by the finite wordlength) improves the performance significantly.

Received Oct. 26, 1993; revision received Feb. 27, 1994; accepted for publication Sept. 22, 1994.

*Research Associate, Space Systems Control Laboratory.

†Research Assistant, Space Systems Control Laboratory. Student Member AIAA.

‡Professor, School of Aeronautics and Astronautics; Director, Space Systems Control Laboratory. Fellow AIAA.

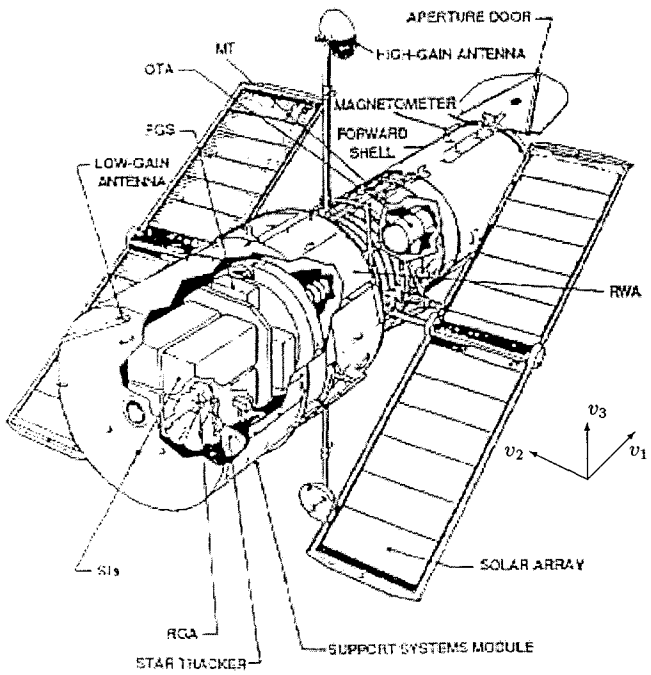

Fig. 1 HST and its vehicle coordinates.

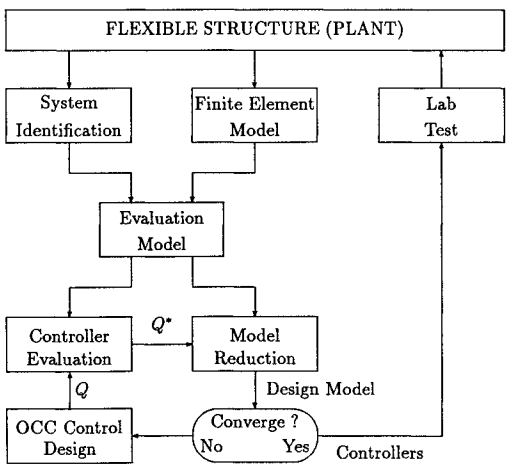

Fig. 2 Block diagram of IMC software.

Model Reduction of Hubble TREETOPS Models

NASA provided three TREETOPS models for the solar array angles at 0, 45, and 105 deg. The frequencies, damping coefficients, and mode shapes vary with the solar array angle. Our model reduction intends to obtain three reduced-order models such that the same appendage (solar panel) frequency modes are captured in each of the three reduced-order models, assuming that the variations of the solar panel model are small.

There exists an optimal realization (called "cost-decoupled" coordinates) of any linear system for model reduction by state truncation. The truncated model obtained by component cost analysis in cost-decoupled coordinates is optimal with respect to the minimal perturbation of the $\mathcal{L}_2$ norm[10] of the output. The modal coordinates are approximately "cost decoupled" when the damping of the system (structure) is very small. This is our motivation for selecting the MCA[11,12] model reduction method. This method decomposes the weighted variance of the output vector y into contributions $\mathcal{V}_i$ of each structural mode as follows:

$$\lim_{t\to\infty} \mathcal{E}_y^T(t)Qy(t) = \sum_{i=1}^{N} \mathcal{V}_i \tag{1}$$

where $\mathcal{E}$ is the expectation operator and Q is a weighting matrix. The TREETOPS models consist of both rigid-body and flexible-structure modes. The MCA determines which modes to retain in an iterative way using the integrated modeling and control (IMC) software.[13] The main idea of the IMC algorithm is shown in Fig. 2. Note that in the IMC iterative process the modes that are important for control influence the modes selected in model reduction. For a physical system, the mathematical model of the given system can be obtained by identification or by mathematical modeling. Then the software starts either with the signals that are necessary for identification or with the given mathematical model. Based on the given model or identified model, this integrated process will produce controllers for evaluation. If the requirements of the evaluation are satisfied, the controllers can be implemented for testing. The IMC algorithm uses the OCC technique for controller design and MCA technique for model reduction. To conduct multimodel reduction, a combined MCA (computing the combined summation of the modal contribution for TREETOPS models with solar angles 0, 45, and 105 deg) is applied in the model reduction process.

To reduce unobservable modes from the evaluation models, a preliminary model reduction using the continuous-time combined MCA technique is applied to the full 120th-order continuous-time TREETOPS models associated with solar array angles 0, 45, and 105 deg. We obtain 80th-order models (called continuous-time evaluation models), where each model contains 3 rigid-body modes and 37 flexible modes (whose mode numbers are 1, 2, 4–12, 14–18, 20–37, 47, 48, and 51). The 80th-order continuous-time evaluation models are discretized at the 40-Hz sample rate, with 0.008 s delay in the control channels to allow the real-time control computer to accomplish the computation of control law. Because of the delay in three control channels, the discrete-time evaluation models have order 83.

The "design models" are reduced-order models used for control design. The IMC algorithm uses an iterative process to provide a design model that is appropriate for the controller with the "best" performance. This iteration is described as follows. First, an initial output weighting matrix Q is given for the MCA model reduction. For the HST control design we used the following weighting matrix:

$$Q = \text{diag}[\,0.1^{-2} \quad 0.007^{-2} \quad 0.007^{-2}\,] \tag{2}$$

which contains the squared inverse of the output specifications (0.007 arc-s about axes v_2 and v_3) in the diagonal elements. The different specification between v_1, v_2, and v_3 is due to the pointing error requirements. The motivation for using the squared inverse of the output specification in Q is that we would like to penalize more the outputs with tight performance requirements. However, this starting choice is not critical since the OCC algorithm finally chooses the weight. The input noise intensity is identity divided by the sampled period ($T_s = 0.025$ s). Reduced-order models (32nd order) with solar angles 0 deg, 45 deg, and 105 deg are obtained by MCA. Second, a sequence of controllers from low control effort to high control effort can be found using the OCC control design technique (calculated using the design model) to satisfy output covariance specifications of the form $\mathcal{E}y_i y_i^T \le \bar{Y}_i\alpha$, where the parameter α is reduced iteratively to guarantee the required performance. Hence, the sequence of controllers has monotonically increasing control effort to satisfy the output constraints. On each iteration, after evaluating the controller with the evaluation ("truth") model, the output weighting matrix Q for MCA is replaced with the Kuhn-Tucker parameters Q_{KT} associated with the inequality constraints in the optimization problem. Reference 14 shows that this optimization yields a linear quadratic Gaussian (LQG) controller that corresponds to the choice $Q = Q_{KT}$ in the LQG cost. At convergence, the maximal accuracy of the closed-loop system combining the evaluation model and the low-order controller can be found. That is, the MCA model reduction and the OCC control design are repeated until the reduced-order model converges. For the HST model reduction, this iterative process converged within three iterations (i.e., the second and third iterations provided the same reduced-order model). During each iteration, 13 modes were kept in the reduced order model (design model). At the first iteration, the modes 8, 6, 7, 5, 1, 2, 12, 17, 18, 4, 15, 11, and 16 (which have the highest combined modal costs) were kept in the reduced-order model, and in the second and third iterations, the modes 8, 6, 7, 2, 5, 1, 12, 16, 17, 18, 4, 15,

Table 1 Combined modal costs and frequencies

Mode number	Combined modal cost (normalized)	Frequencies of solar array angles, Hz			Maximum change of frequency between models, %
		0 deg	45 deg	105 deg	
8	4.625×10^{1}	0.1123	0.1132	0.1205	6.8
6	2.467×10^{1}	0.1110	0.1109	0.1004	9.6
7	1.706×10^{1}	0.1115	0.1117	0.1016	9.9
2	5.507×10^{0}	0.0127	0.0127	0.0127	0
5	4.137×10^{0}	0.1100	0.1100	0.0912	17.9
1	1.561×10^{0}	0.0126	0.0126	0.0126	0
12	2.700×10^{-1}	0.2855	0.2857	0.3168	9.9
16	1.804×10^{-1}	0.4657	0.4549	0.5421	16.9
17	1.484×10^{-1}	0.5301	0.5301	0.5603	5.7
18	8.657×10^{-2}	0.5304	0.5307	0.6644	20.2
4	3.475×10^{-2}	0.0200	0.0200	0.0200	0
15	3.243×10^{-2}	0.4322	0.4319	0.5414	22.1
10	1.671×10^{-2}	0.1900	0.1901	0.2266	16.2
11	1.290×10^{-2}	0.2852	0.2852	0.3159	9.7
33	9.260×10^{-3}	1.0888	1.0937	1.0976	0.8
22	6.263×10^{-3}	0.7402	0.7404	0.7640	3.1

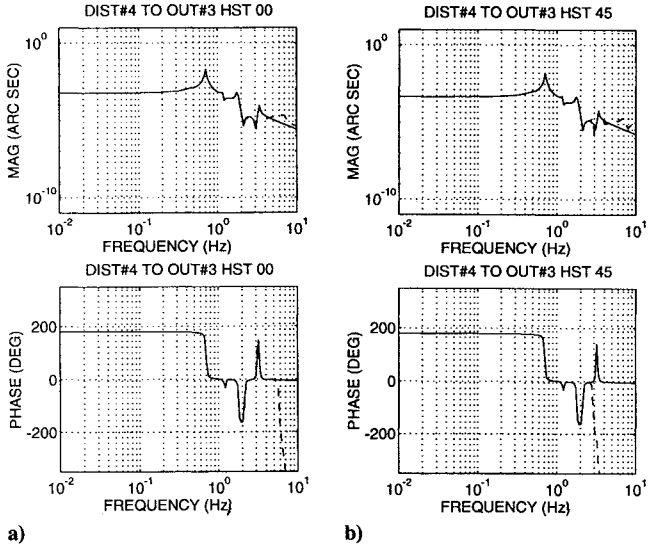

Fig. 3 Frequency response comparison of full and design models. Dashed line: 120th-order TREETOPS models. Solid line: 32nd-order design models.

and 10 were kept. Hence, mode 11 was replaced by mode 10 in the second and third iterations. The MCA results of the second iteration are presented in Table 1.

In order to check the quality of the model reduction by open-loop standards (we do not use open-loop information in the final selection of the models because a good match on the open-loop frequency responses does not necessarily lead to a good design model), the frequency responses of the full-order TREETOPS models and the reduced-order models (design models) are plotted in Fig. 3. The frequency responses match well for the frequency range below 2 Hz. For example, Fig. 3a provides the frequency responses of the full-order TREETOPS model and the reduced-order design model from disturbance channel 4 to vehicle axis v_3 for solar panel angle 0 deg. Figure 3b provides the frequency responses of the full-order TREETOPS model and the reduced-order design model associated with solar panel angle 45 deg from disturbance channel 6 to vehicle axis v_3.

Controller Design Using Integrated Modeling and Control Algorithm

The design strategy used in this section is to integrate the modeling and the control design using the IMC software[13] developed at the SSCL at Purdue. We follow an iterative approach that takes into account the interdependence of the model reduction and the controller design procedures. We design an OCC controller using the 32nd-order design model discussed in the previous section. In order to compensate the bias torques produced by gravity, two proportional-integral (PI) filters with the discrete transfer function

$$g(z) = (z - 0.98)/(z - 1) \tag{3}$$

are serially connected to the measurement channels corresponding to the vehicle coordinates v_2 and v_3. Hence, the order of the design model is increased to 34. The corresponding controllers designed based upon the 34th-order design model have order 34. After combining the 34th-order controller with the two first-order filters, described by Eq. (3), the OCC controller has order 36.

The OCC algorithm[14] is applied for controller design. The linear discrete time-invariant system is written as

$$\begin{aligned} x(k+1) &= Ax(k) + Bu(k) + Dw_p(k) \\ y(k) &= Cx(k) \\ z(k) &= Mx(k) + v(k) \end{aligned} \tag{4}$$

where x, y, z, u, w_p, and v are the vectors of state, output, measurement, system disturbance, and measurement noise, respectively. We assume that the output y has the form $y^T = [y_1^T, y_2^T, \ldots, y_m^T]$ and that $w_p(\cdot)$ and $v(\cdot)$ are zero-mean white noises with covariances $\mathcal{E}\{w_p(\cdot)w_p^T(\cdot)\} = W_p$ and $\mathcal{E}\{v(\cdot)v^T(\cdot)\} = V$, respectively.

The OCC problem is the following: Find a full-order proper dynamic controller

$$\begin{aligned} x_c(k+1) &= A_c x_c(k) + B_c z(k) \\ u(k) &= C_c x_c(k) + D_c z(k) \end{aligned} \tag{5}$$

to minimize $J = \lim_{k\to\infty} \mathcal{E}u^T(k)Ru(k)$ subject to the inequality covariance constraints

$$\lim_{k\to\infty} \mathcal{E}y_i(k)y_i^T(k) \triangleq Y_i \le \bar{Y}_i, \qquad i = 1, 2, \ldots, m \tag{6}$$

where R is a given positive-definite weighting matrix. The OCC problem can be solved using the OCC algorithm,[14] which has guaranteed convergence and global optimality.

To apply the OCC design algorithm for the HST controller design, we consider the HST TREETOPS models where the three outputs $\hat{y}_1$, $\hat{y}_2$, $\hat{y}_3$ represent the angles about the vehicle axes v_1, v_2, and v_3. These outputs are divided into two groups y_1 and y_2, where $y_1 = \hat{y}_1$ and $y_2^T = [\hat{y}_2, \hat{y}_3]^T$. The output covariance constraint-bound matrices we consider have the form $\bar{Y}_i = \sigma_i I, i = 1, 2$. To understand the physical interpretation of the OCC problem, consider, for example, the constraint $\lim_{k\to\infty} \mathcal{E}y_2(k)y_2^T(k) \le \sigma_2 I_2$, where I_2 is the 2×2

identity matrix. The results on the l_2-to-l_∞ gain of a system obtained in Ref. 17 guarantee that, in the presence of any l_2 (bounded energy) disturbances w_p and v, the peak magnitude of the time response of the output $\|y_2(\cdot)\|_\infty$ is bounded as follows:

$$\|y_2(\cdot)\|_\infty^2 \le \sigma_2 \left\| \left[w_p^T(\cdot) v^T(\cdot) \right] \right\|_2^2 \tag{7}$$

Hence, if $\|[w_p^T(\cdot)v^T(\cdot)]\|_2^2 = 1$ (i.e., the input disturbance has unit l_2 norm), then the pointing error in the v_2–v_3 plane is guaranteed to be bounded by σ_2. Therefore, we choose the bounds σ_1 and σ_2 as our design specification for the HST PCS. Note that the actual HST disturbance need not be known in order to bound the pointing error y. One only needs an upper bound on the l_2 norm (the energy) of the disturbances.

The 83rd-order evaluation models associated with the solar array angles at 0 deg, 45 deg, and 105 deg are used to evaluate our reduced-order (36th-order) controller. Minimal reachable performance bounds σ_i^m with respect to the design models are calculated by the iterative model-design-evaluate procedure in the IMC algorithm. The OCC design specification should not be smaller than the maximal accuracy associated with the current model. Hence, σ_i is expressed as a function of an integer α (the performance tuning parameter) as follows[14]:

$$\sigma_i(\alpha) = (1-\gamma)^\alpha \left(\sigma_i^o - \sigma_i^m\right) + \sigma_i^m, \qquad \alpha = 1, 2, \ldots, n \tag{8}$$

where $0 \le \gamma \le 1$ is a free parameter to be chosen, σ_i^o are the initial constraints, and σ_i^m are the maximal accuracies (the lower bounds of the achievable specifications for design models). By iterating on α (hence we call this the "α study"), the best performance can be obtained for the evaluation model, whereas the design is based upon the design model.

We designed the OCC controllers using the 34th-order reduced-order models associated with the solar array angles at 0 deg, 45 deg, and 105 deg. It turns out that the controller based on the reduced-order model associated with solar panel angle at 0 deg provides the single best controller performance over the three evaluation models associated with solar array angles at 0 deg, 45 deg, and 105 deg. Hence, the OCC α-study control design is based on the reduced-order design model of solar panel angle at 0 deg. We choose the control weighting matrix R to be identity. The noise covariance matrices used for the OCC design are

$$W_p = I_{12}/T_s, \qquad V = I_3(0.000125)^2/T_s \tag{9}$$

where I_k is the $k \times k$ identity matrix, $T_s = 0.025$ s is the sample period, and 0.000125 is the resolution of the rate gyros. The design specifications σ_i vary according to Eq. (8), where $\gamma = 0.2$ and

$$\sigma_1^o = \sigma_1^m = 4.27 \times 10^{-6}, \qquad \sigma_2^o = 5.98 \times 10^{-6}$$
$$\sigma_2^m = 5.98 \times 10^{-8} \text{ arc-s}^2 \tag{10}$$

Since we choose $\sigma_1^o = \sigma_1^m$, the maximal singular-value constraint on the covariance of the first output group is fixed (4.27×10^{-6}), and the constraint on the covariance of the second output group (v_2–v_3 plane) reduces as the parameter α increases. In fact, in the α study we are trying to find (numerically) the best performance of the second output group, which can be obtained by the OCC controller. Each controller designed in the a study is evaluated with the 83rd-order evaluation models associated with the solar panel angles at 0, 45, and 105 deg. The maximal singular values of the covariances of the second output group of each closed-loop system are plotted in Fig. 4 for $\alpha = 1, 2, \ldots, 20$. The values of these maximal singular values are approximately the same for the closed-loop systems associated with solar panel angles at 0 deg, 45 deg, and 105 deg, but the required control efforts [$J = \lim_{k\to\infty} \mathcal{E} u^T(k)u(k)$] are quite different due to modeling errors (note that all controllers shown are designed based on the model associated with the solar panel angle at 0 deg). Note especially that for the maximal singular value of the closed-loop covariance associated with the solar angle at 105 deg, when $\alpha > 10$, a small reduction on the maximal singular value causes a large increase in the control effort. To obtain the best performance, the 20th controller (called the OCC controller in the rest of this paper) of the α study is used for the design evaluation.

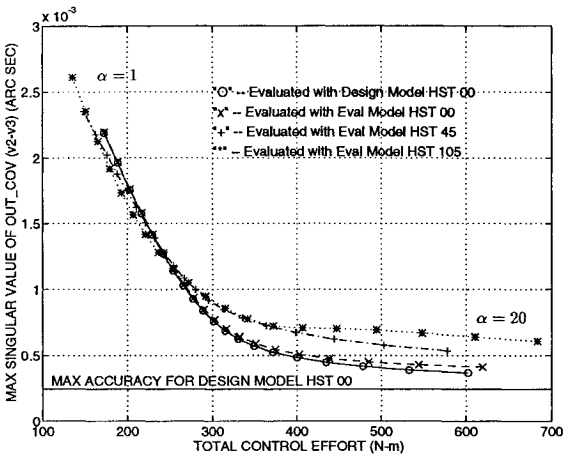

Fig. 4 Performance tuning of OCC design based on HST 00.

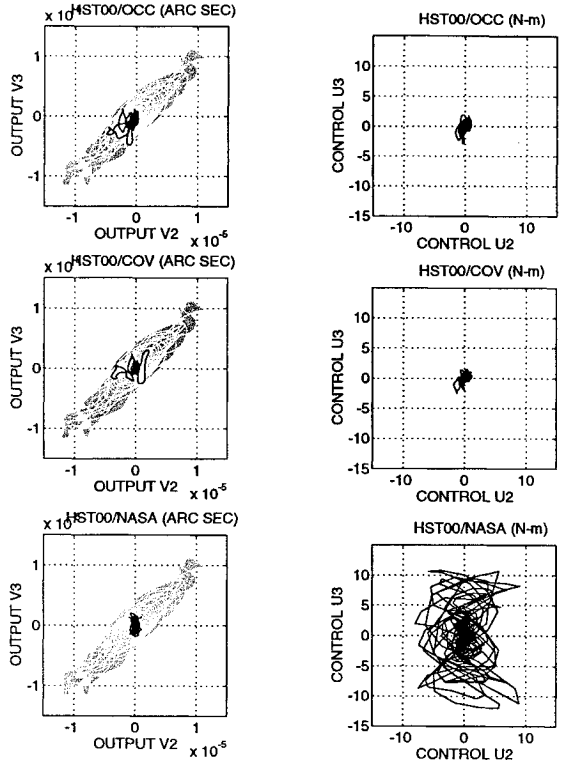

Fig. 5 Open/closed-loop responses of OCC, COV, and NASA controllers. Left figures: solid line, closed-loop responses; shaded area, open-loop responses. Right figures: closed-loop control signals.

Figure 5 provides the pulse responses of the open- and closed-loop systems associated with solar panel at 0 deg for the OCC, covariance (COV), and NASA (SAGA-II) controllers, where the COV controller will be discussed later. The open-loop models used for simulations are the 83rd-order evaluation models associated with solar panel angles 0 deg, 45 deg, and 105 deg. The closed-loop systems are formed with either the OCC controller or the NASA controller and the 83rd-order evaluation models. The pulse input signals suggested by NASA for this simulation have the following magnitude:

$$w_p(0) = [-1 \quad -0.98 \quad 1.02 \quad 0.97 \quad -0.99 \quad -0.97 \quad 0.980.99 \quad 0 \quad 0 \quad 0 \quad 0]^T \text{ N-m} \tag{11}$$

From Fig. 5, it is clear that a large improvement of the rms values of the outputs is obtained for the evaluation models associated with

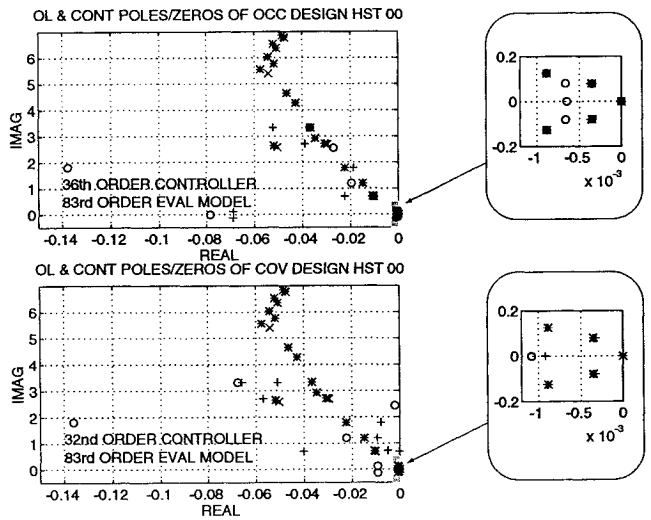

Fig. 6 Open-loop and OCC/COV controller pole/zero positions: ∗, open-loop poles; ×, open-loop zeros; +, controller poles; ○, controller zeros.

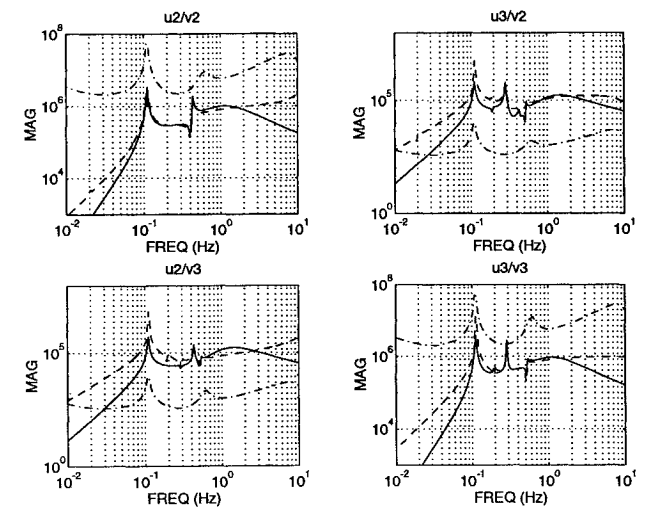

Fig. 7 Frequency responses of OCC, COV, and NASA controllers. Solid line: 36th-order OCC controller. Dashed line: 32nd-order COV controller. Dashdot line: 28th-order NASA controller.

solar panel angles at 0 deg by both the NASA controller and the OCC controller. The simulation results shown in Fig. 5 will be discussed later.

The closed-loop pointing errors of the OCC controller and NASA controller are approximately equal (the pointing error of the NASA controller is slightly smaller than the OCC controller for this simulation). However, the control magnitude of the NASA controller is almost 10 times larger than that of the OCC controller. This result is not surprising since the objective of the OCC controller is to minimize the control effort. The pointing errors with linear simulation at the solar panel angles 45 deg and 105 deg are similar to the case at the solar panel angle 0 deg.

The open-loop and controller poles and zeros are plotted in Fig. 6. The discrete-time controller is mapped to the continuous-time domain, and the poles and zeros are computed. It is obvious that the controller has some zeros near the 0.1-, 0.2-, and 0.6-Hz open-loop poles, indicating that the controller is trying to reduce the effect of these open-loop poles by placing zeros nearby. The frequency responses of the controller from the second and third control channels to the second output group (v_2, v_3) are plotted in Fig. 7.

The open- and closed-loop frequency responses of the OCC and NASA controllers are plotted in Fig. 8. It is clear that the magnitude of the NASA controller at the low-frequency area (10^{-2}–10^{-1}) is much smaller than that of the OCC controller, which might explain

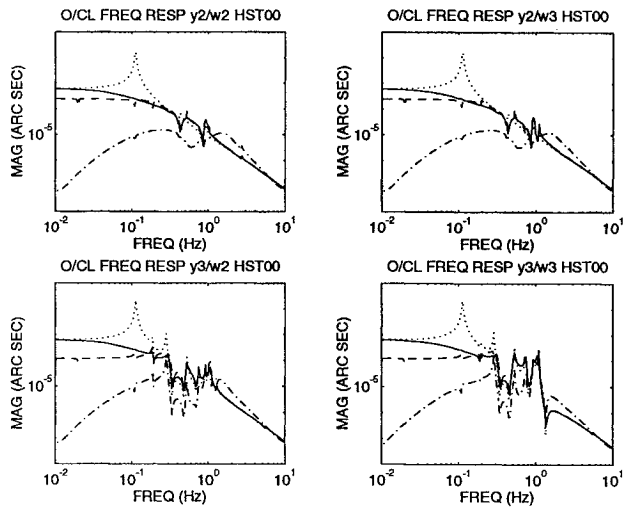

Fig. 8 Closed-loop frequency responses of OCC, COV, and NASA controllers. Dotted line: Open loop. Solid line: 36th-order OCC controller. Dashed line: 32nd-order COV controller. Dash-dot line: 28th-order NASA controller.

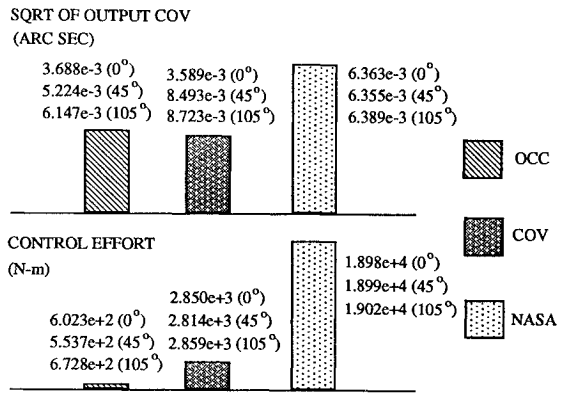

Fig. 9 OCC, COV, and NASA controller comparison.

why the control effort of the NASA controller is one order higher than for the OCC controller. The closed-loop output covariances and input variances (control energies) of the OCC and NASA controllers are compared in Fig. 9.

Covariance Control Design

Covariance control theory provides a characterization of all assignable covariance matrices and, in addition, a parametrization of all controllers that assign a particular assignable covariance. Using these tools, the covariance control design problem is based on these three steps:

1) Formulate the assignability conditions and the desired performance objectives as constraints in the space of covariance matrices.

2) Use numerical techniques to obtain an assignable covariance that satisfies the constraints of step 1.

3) Obtain a satisfactory controller from the parametrization of all controllers that assigns the desired covariance computed in step 2.

Hence, the covariance control theory formulates the control design problem in the space of covariance parameters instead of the space of controller parameters. Output covariance constraints can be satisfied by appropriately constraining the state covariance matrix in step 2. In addition, by proper selection of the controller covariance matrix we can scale the controller states to satisfy digital implementation constraints using fixed-point arithmetic.[2]

The covariance control formulation provides desirable properties like convexity. The alternating convex projection (ACP) techniques[8,16] were suggested to provide solutions to step 2. Following the geometric approach,[16] the covariance design problem is formulated as a feasibility problem to find a discrete plant covariance matrix X_p to lie in the intersection of certain closed convex sets that correspond to assignability and performance constraints.

All stabilizing controllers of order equal to or less than the plant must have covariances in the two convex sets $\mathcal{A}$ and $\mathcal{P}$:

$$\mathcal{A} = \{X_p : (I - BB^+)(AX_pA^T - X_p + DW_pD^T) \times (I - BB^+) = 0\} \tag{12}$$

$$\mathcal{P} = \{X_p : X_p \geq P\} \tag{13}$$

where $[\cdot]^+$ denotes the Moore-Penrose generalized inverse of $[\cdot]$ and P is the positive-definite solution of the following Riccati equation:

$$P = APA^T - APM^T(V + MPM^T)^{-1}MPA^T + DWD^T \tag{14}$$

The constraint sets we consider for the HST controller design are the two assignability constraint sets $\mathcal{A}$ and $\mathcal{P}$. The performance constraint sets are also convex in X (see Ref. 16 for proof),

$$\mathcal{V}_1 = \{X_p : \bar{\sigma}[Y_1] \leq \sigma_1\} \tag{15}$$

$$\mathcal{V}_2 = \{X_p : \bar{\sigma}[Y_2] \leq \sigma_2\} \tag{16}$$

where Y_1 and Y_2 are the (1, 1) and (2, 2) blocks of the output covariance matrix, respectively, corresponding to the outputs y_1 and the outputs $\hat{y}_2$ and $\hat{y}_3$. The output covariance performance constraints were chosen to be (in square arcseconds)

$$\sigma_1 = 4.3 \times 10^{-6}, \qquad \sigma_2 = 1.3 \times 10^{-7} \tag{17}$$

The reduced-order model used for design is the 32nd-order discrete-time model described earlier without the filters given in Eq. (3).

The first two sets $\mathcal{A}$ and $\mathcal{P}$ correspond to assignability constraints and the sets $\mathcal{V}_i$ are the desired output variance constraints. Hence, we look for a plant covariance matrix X_p in the intersection of these sets. Application of the directional ACP algorithm described in Ref. 16 provides an assignable covariance matrix such that the desired performance constraints are satisfied. The algorithm converges in 738 iterations for an error tolerance of 1.0×10^{-10}. The closed-loop covariance matrix X is assembled such that the controller state covariance matrix X_c is equal to identity. (This choice meets a scaling constraint for finite-wordlength computation,[2] but otherwise roundoff was not treated in this design.)

Covariance control theory provides an analytic expression for all controllers that assign the designed covariance to the closed-loop system. The set of all controllers that assign the closed-loop covariance X to the closed-loop system is a function of the plant matrices, the closed-loop covariance, and a free unitary matrix U, i.e.,

$$\{A_c, B_c, C_c, D_c\} = F(A, B, C, D, M, X, U) \tag{18}$$

The explicit formulas of (18) can be found in Ref. 4. We choose the unitary freedom U such that the control effort required to assign the closed-loop covariance X is minimized. This choice of U is provided by an analytical expression derived in Ref. 17.

The output variances of the closed-loop system were found to be the following [which can be compared to specifications in Eq. (17)]:

$$\sigma_1 = 4.2814 \times 10^{-6}, \qquad \sigma_2 = 1.2886 \times 10^{-7} \tag{19}$$

Figure 7 provides the frequency response plots of the designed controller from the second and third control channels to the second and third outputs (v_2, v_3). Note that both the covariance controller and the OCC controller have similar gains at the 0.1-Hz elastic mode and the 0.6-Hz elastic mode. Figure 6 provides the locus of open-loop poles and covariance controller poles and zeros in the continuous-time domain. The pulse response of the closed-loop system is provided in Fig. 5 for the pulse signal given in Eq. (11). Figure 6 shows the pulse response for solar array angle at 45 deg.

Finite-Wordlength Effects

The finite-wordlength implementation of a controller in a digital computer can drastically affect the performance of the control system.[2] There exist realizations of a given controller yielding arbitrary large effects from computational errors. On the other hand, there exist realizations so that the finite-wordlength computational errors are minimized. To demonstrate the importance of these finite-wordlength implementation effects, this section evaluates the performance of controllers designed for the HST for a wide range of control computer wordlengths. In addition, we compute for each controller an optimal coordinate transformation to minimize these finite-wordlength effects. We propose here a methodology for any space flight using a fixed-point computer. The application to HST will give insight into the role played by the wordlengths. This would certainly be useful in future missions requiring a controller of low complexity (memory).

The three controllers to be evaluated for finite-wordlength implementation are the 36th-order controller designed using the IMC algorithm, the 32nd-order covariance controller designed using the ACP algorithm, and the NASA SAGA-II controller provided by NASA. The evaluation model is the 83rd-order model described in the model reduction section.

Figure 10 shows the variation of the control effort vs the maximum singular value of the covariance of the outputs (v_2, v_3) for different values of the control computer wordlength. This finite-wordlength performance evaluation is provided for the three controllers: the OCC controller, the covariance controller (denoted by COV), and the NASA controller. The infinite-wordlength performance of these correspond to the points denoted by $\beta = 36$. However, this performance will not be achieved when the controllers are implemented in a finite-wordlength control computer. We have evaluated this performance degradation for control computer wordlength varying from $\beta = 4$ to $\beta = 36$. The points denoted by circles correspond to the performance evaluation in the design coordinates. There are three curves that correspond to the three controllers for evaluation. The control computer wordlength varies in these curves from $\beta = 4$ bits to $\beta = 36$ bits with intermediate steps of 2 bits (The HST computer has 24 bits). It can be seen that the decrease of the computer wordlength has a significant degradation in the controller performance. The finite-wordlength implementation has less effect on the covariance controller, and this is attributed to the fact that the covariance controller is capable of scaling the states of the controller such that $X_c = I$; i.e., the controller state covariance matrix is chosen to be the identity. Note that the significant effect of the finite-wordlength implementation in this problem is due to the large magnitude of the roundoff noise (relative to the measurement noise) when the number of available control computer bits is small.

For each of the two controllers discussed above, an optimal transformation is computed to minimize the roundoff noise subject to unity l_2-norm scaling constraints on the diagonal elements of the controller covariance. This optimal coordinate transformation is described in Ref. 2. We call these controllers OCC_{FW}, COV_{FW}, and

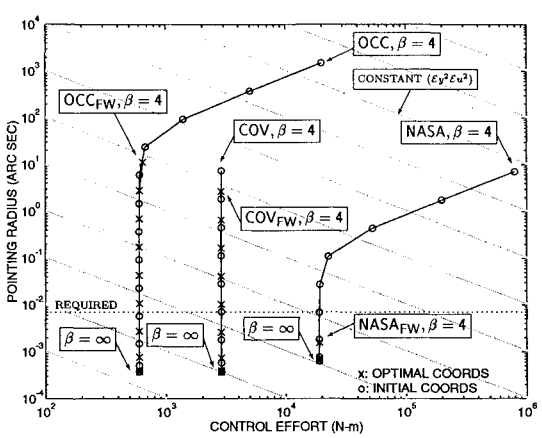

Fig. 10 Finite-wordlength (β-bit) evaluation of *OCC*, *COV*, *NASA*, OCC_{FW}, COV_{FW}, and $NASA_{FW}$ controllers.

$NASA_{FW}$. The evaluation of the controllers in these optimal coordinates is provided in Fig. 10 (points denoted by crosses). Again the evaluation ranges for computer wordlength from $\beta = 4$ to $\beta = 36$ bits. As expected, for large wordlengths, there is no distinction between the performance of the controllers in the initial coordinates and the optimal coordinates. However, for short wordlengths the optimal transformation can provide a significant improvement in the pointing error accuracy. For example, for the OCC controller and a 12-bit control computer, there is an improvement of more than two orders of magnitude with almost no additional control effort. The justification for taking the finite wordlength into consideration in the controller design is the ability to trade closed-loop performance (rms values) vs computer resources (wordlengths). These tools can help with computer design requirements in future missions. For example, Fig. 10 shows that the NASA controller could meet the design requirements using a 14-bit wordlength, whereas the COV and OCC controllers need 14 and 22 bits respectively. Using the optimal realization the $NASA_{FW}$, COV_{FW}, and OCC_{FW} controllers need, respectively, 4, 14, and 16 bits.

Conclusion

An IMC algorithm is applied for HST controller redesign yielding a 36th-order centralized controller whose performance is evaluated using three 83rd-order evaluation models associated with solar panel angles 0, 45, and 105 deg. Six controllers are evaluated, *OCC*, OCC_{FW}, *COV*, COV_{FW}, *NASA*, and $NASA_{FW}$, where the subscript FW denotes optimal state-space realization of the controller to minimize roundoff due to finite-wordlength effects. The OCC controller minimizes the control energy with a specified upper bound on the output covariance. The *COV* controller assigns a desirable state covariance matrix to the closed-loop system. The OCC_{FW} and COV_{FW} controllers have the main advantage of low control energy compared to the *NASA* controller.

A special feature of the paper is the minimization of roundoff error and the technique to trade closed-loop dynamic response performance with computer wordlength. To note this effect, for instance, the NASA controller could meet the performance specification with just 4 bits using the optimal controller realization, but in the coordinates in which it was implemented it needs 14 bits to yield the same performance. Our finite-wordlength controller design techniques allow a tradeoff between output performance and the total controller resources: the control energy and the controller complexity (memory, as measured by the total of all wordlengths). The ability to trade performance with computer resources could be important in future missions and allows the specifications on the computer hardware design to be tailored more efficiently to the actual required performance of the system.

Acknowledgment

This research was supported by NASA Grant NAG8-930.

References

[1]Sharkey, J., Nurre, G., Beals, G., and Nelson J., "A Chronology of the On-Orbit Pointing Control System Changes on the Hubble Space Telescope and Associated Pointing Improvement," *Proceedings of the AIAA Guidance, Navigation, and Control Conference* (Hilton Head Island, SC), AIAA, Washington, DC, 1992, pp. 1418–1433; also AIAA Paper 92-4618.

[2]Liu, K., Skelton, R., and Grigoriadis, K., "Optimal Controllers for Finite Wordlength Implementation," *IEEE Transactions on Automatic Control*, Vol. 37, No. 9, 1992, pp. 1294–1304.

[3]Hotz, A., and Skelton R. E., "Covariance Control Theory," *International Journal of Control*, Vol. 46, No. 1, 1987, pp. 13–32.

[4]Iwasaki, T., and Skelton, R. E., "A Computational Algorithm for Covariance Control: Continuous-Time Case," *Proceedings of the Allerton Conference* (Monticello, IL), Sept. 1992, pp. 267–276.

[5]Skelton, R. E., and Ikeda, M., "Covariance Controllers for Linear Continuous-Time Systems," *International Journal of Control*, Vol. 49, No. 5, 1989, pp. 1773–1785.

[6]Yasuda, K., Skelton, R. E., and Grigoriadis, K., "Covariance Controllers: A New Parameterization of the Class of All Stabilizing Controllers," *Automatica*, Vol. 29, No. 3, 1993, pp. 785–788.

[7]Liu, K., Skelton, R. E., and Sharkey, J. P., "Modeling Hubble Space Telescope Flight Data by q-Markov Cover Identification," *Proceedings of the American Control Conference* (Chicago, IL), June 1992, pp. 1961–1966.

[8]Grigoriadis, K. M., and Skelton, R. E., "Alternating Convex Projection Method for Covariance Control Design," *Proceedings of the Allerton Conference* (Monticello, IL), Sept. 1992, pp. 88–97.

[9]Mullis, C., and Roberts, R., "Synthesis of Minimum Round-off Noise Fixed Point Digital Filters," *IEEE Transactions on Circuits and Systems*, Vol. 23, 1976. pp. 551–562.

[10]Skelton, R. E., *Dynamic Systems Control: Linear Systems Analysis and Synthesis*, Wiley, New York, 1988.

[11]Skelton, R. E., Singh, R., and Ramakrishnan, J., "Component Model Reduction by Component Cost Analysis," *Proceedings of the AIAA Guidance, Navigation, and Control Conference* (Minneapolis, MN), AIAA, Washington, DC, 1988, pp. 264–274; also AIAA Paper 88-4086.

[12]Kim, J. K., and Skelton, R. E., "Model Reduction by Weighted Component Cost Analysis," *Proceedings of the Dynamics Specialist Conference* (Long Beach, CA), AIAA, Washington, DC, 1990, pp. 153–160; also AIAA Paper 90-1207.

[13]Zhu, G., and Skelton, R. E., "Integrated Modeling and Control for the Large Spacecraft Control Laboratory Experiment Facility," *Journal of Guidance, Control, and Dynamics*, Vol. 17, No. 3, 1994, pp. 442–450.

[14]Zhu, G., Rotea, M., and Skelton, R. E., "A Convergent Feasible Algorithm for the Output Covariance Constraint Problem," *Proceedings of the 1993 American Control Conference* (San Francisco, CA), June 1993, pp. 1675–1679.

[15]Grigoriadis, K. M., Skelton, R. E., and Frazho, A. E., "Alternating Convex Projection Methods for Discrete-Time Covariance Control," *Proceedings of the IEEE Conference on Decision and Control* (San Antonio, TX), Dec. 1993, pp. 1782–1786.

[16]Grigoriadis, K., and Skelton, R. E., "Minimum Effort Covariance Controllers," *Proceedings of the IEEE Conference on Decision and Control* (San Antonio, TX), Dec. 1993, pp. 823–824.

[17]Zhu, G., Corless, M., and Skelton, R., "Robustness Properties of Covariance Controllers," *Proceedings of the Allerton Conference* (Monticello, IL), Sept. 1989, pp. 877–883.